*Inorg. Chem.* **2005**, *44*, 4656–4665


# Structural and Photophysical Properties of Coordination Networks Combining $[Ru(bipy)(CN)_4]^{2-}$ Anions and Lanthanide(III) Cations: Rates of Photoinduced Ru-to-Lanthanide Energy Transfer and Sensitized Near-Infrared Luminescence

**Graham M. Davies,[†] Simon J. A. Pope,[‡] Harry Adams,[†] Stephen Faulkner,*[,‡] and Michael D. Ward*[,†]**

*Department of Chemistry, University of Sheffield, Sheffield S3 7HF, United Kingdom, and Department of Chemistry, University of Manchester, Oxford Road, Manchester M13 9PL, United Kingdom*

Received April 5, 2005

Co-crystallization of $K_2[Ru(bipy)(CN)_4]$ with lanthanide(III) salts (Ln = Pr, Nd, Gd, Er, Yb) from aqueous solution affords coordination oligomers and networks in which the $[Ru(bipy)(CN)_4]^{2-}$ unit is connected to the lanthanide cation via Ru–CN–Ln bridges. The complexes fall into two structural types: $[\{Ru(bipy)(CN)_4\}_2\{Ln(H_2O)_m\}\{K(H_2O)_n\}]\cdot xH_2O$ (Ln = Pr, Er, Yb; $m$ = 7, 6, 6, respectively), in which two $[Ru(bipy)(CN)_4]^{2-}$ units are connected to a single lanthanide ion by single cyanide bridges to give discrete trinuclear fragments, and $[\{Ru(bipy)(CN)_4\}_3\{Ln(H_2O)_4\}_2]\cdot xH_2O$ (Ln = Nd, Gd), which contain two-dimensional sheets of interconnected, cyanide-bridged $Ru_2Ln_2$ squares. In the Ru–Gd system, the $[Ru(bipy)(CN)_4]^{2-}$ unit shows the characteristic intense $^3$metal-to-ligand charge transfer luminescence at 580 nm with $\tau$ = 550 ns; with the other lanthanides, the intensity and lifetime of this luminescence are diminished because of a Ru → Ln photoinduced energy transfer to low-lying emissive states of the lanthanide ions, resulting in sensitized near-infrared luminescence in every case. From the degree of quenching of the Ru-based emission, Ru → Ln energy-transfer rates can be estimated, which are in the order Yb ($k_{EnT} \approx 3 \times 10^6$ sec$^{-1}$, the slowest energy transfer) < Er < Pr < Nd ($k_{EnT} \approx 2 \times 10^8$ sec$^{-1}$, the fastest energy transfer). This order may be rationalized on the basis of the availability of excited f–f levels on the lanthanide ions at energies that overlap with the Ru-based emission spectrum. In every case, the lifetime of the lanthanide-based luminescence is short (tens/hundreds of nanoseconds, instead of the more usual microseconds), even when the water ligands on the lanthanide ions are replaced by $D_2O$ to eliminate the quenching effects of OH oscillators; we tentatively ascribe this quenching effect to the cyanide ligands.

## Introduction

Near-infrared (NIR) luminescence from lanthanides such as Yb(III), Er(III), Pr(III), and Nd(III) has become an area of intense interest in the past few years because of its relevance to applications as diverse as luminescent probes for use in biological media and optical amplification in fiber-optic telecommunications systems.[1,2] Very often, ligand-centered $\pi-\pi^*$ transitions in the UV region have been used to sensitize lanthanide luminescence following a ligand-to-metal energy transfer; this overcomes the problem that f−f transitions are very weak, so direct excitation is difficult. However, d-block complexes with strong charge-transfer transitions are emerging as effective sensitizer units, for a variety of reasons.[3−5] The high extinction coefficients associated with fully allowed charge-transfer transitions means efficient absorption by the light-harvesting unit; relatively long-lived excited states mean that an energy transfer to the lanthanide ions can occur before the excited state collapses; the wide tunability of metal-to-ligand charge-transfer (MLCT) transitions by varying the metal ion, ancillary ligands, and the ligand substituents means that a sensitizing chromophore can be chosen to have an ideal

* Author to whom correspondence should be addressed. E-mail: m.d.ward@sheffield.ac.uk.
[†] University of Sheffield.
[‡] University of Manchester.

(1) (a) Faulkner, S.; Matthews, J. L. In *Comprehensive Coordination Chemistry*, 2nd ed.; Ward, M. D., Ed.; Elsevier: Oxford, U. K., 2004; Vol. 9, p 913 and refs therein. (b) Tanabe, S. *Compt. Rend. Chim.* **2002**, *5*, 815. (c) Kumar, G. A.; Riman, R.; Snitzer, E.; Ballato, J. *J. Appl. Phys.* **2004**, *95*, 40.



10.1021/ic050512k CCC: $30.25 
Published on Web 05/28/2005

excited-state energy content to match with the energy-receiving level on the lanthanide ion; and the broad luminescence bands characteristic of d-block luminophores maximize the necessary spectral overlap with the sharp, weak lanthanide f−f absorption bands.

In the past few years, the study of the photophysical properties of d−f dyads showing NIR luminescence from the lanthanide has grown rapidly. In a seminal paper, Van Veggel and co-workers used $[Ru(bipy)_3]^{2+}$ and ferrocenyl units as energy donors to Yb(III) and Nd(III), in complexes based on elaborate bridging ligands;[3] the metal−metal separation and lack of a conjugated pathway between the metal centers meant that the energy transfer to the lanthanide was, however, relatively slow. Since then, related examples have been described by a few other groups, with the general theme being the same, namely, that d-block units that absorb in the visible region can effectively sensitize NIR luminescence from attached lanthanide(III) ions,[4,5] and a variety of carefully designed bridging ligands has been used to provide different donor sites for the transition-metal (soft) and lanthanide (hard) sites.[4] Our contribution has involved the use of mononuclear d-block complexes based on potentially bridging ligands such as bipyrimidine and 2,3-bis(2-pyridyl)-pyrazine, containing vacant, externally directed *N,N*-bidentate sites. The addition of lanthanide tris-diketonate units to the secondary site results in d−f dyads with short metal−metal separations and an unsaturated bridging ligand, both of which make d → f energy transfers fast and efficient.[5]

In this paper, we present a different approach and show how co-crystallization of the anionic cyanometalate chromophore $[Ru(bipy)(CN)_4]^{2-}$ with various lanthanide(III) salts results in cyanide-bridged d−f coordination networks, which show sensitized lanthanide luminescence in the NIR region following excitation of the Ru-based MLCT transition. The choice of $[Ru(bipy)(CN)_4]^{2-}$ as the d-block component[6] follows from simple synthetic and photophysical considerations. The negative charge of $[Ru(bipy)(CN)_4]^{2-}$ means that it will co-crystallize with lanthanide cations, and the resulting Ru−CN−Ln bridges are necessarily short and unsaturated. The broad emission spectrum (maximizing donor−acceptor overlap) and relatively long $^3$MLCT lifetime of $[Ru(bipy)(CN)_4]^{2-}$ will both facilitate a d → f energy transfer, as described above.

Indeed, many other cyanometalate units have been used for similar reasons to form cyanide-bridged coordination networks with lanthanide cations.[7−10] Shore and co-workers have prepared and structurally characterized an extensive range of coordination networks based on anionic cyanometalates of *inter alia* Ni(II), Pd(II), Pt(II), and Cu(I).[7] Patterson and co-workers have prepared coordination networks of Eu(III) and Tb(III) with $[Au(CN)_2]^-$ and $[Ag(CN)_2]^-$, which display sensitized luminescence from the lanthanides in the visible region, which is possible because of the high energies (UV region) of the excited states of $[Au(CN)_2]^-$ and $[Ag(CN)_2]^-$.[8] Cyanide-bridged d−f networks have also been extensively studied by others for their magnetic[9] and structural[10] properties.

We describe here the preparation and structural characterization of the coordination networks generated by crystallization of $[Ru(bipy)(CN)_4]^{2-}$ with $Nd^{3+}$, $Pr^{3+}$, $Yb^{3+}$, $Er^{3+}$, or $Gd^{3+}$ ions in water or $D_2O$. Two major structural types, quite different from one another, are observed. The photophysical properties of the resulting solids are described with an emphasis on the sensitized lanthanide luminescence. A small part of this work was recently described in a preliminary communication.[11]


(2) Representative recent papers describing NIR luminescence from lanthanide complexes: (a) Beeby, A.; Burton-Pye, B. P.; Faulkner, S.; Motson, G. R.; Jeffery, J. C.; McCleverty, J. A.; Ward, M. D. *J. Chem. Soc., Dalton Trans.* **2002**, 1923. (b) Hebbink, G. A.; Klink, S. I.; Grave, L.; Oude Alink, P. G. B.; van Veggel, F. C. J. M. *Chem. Phys. Chem.* **2002**, *3*, 1014. (c) Faulkner, S.; Pope, S. J. A. *J. Am. Chem. Soc.* **2003**, *125*, 10526. (d) Magennis, S. W.; Ferguson, A. J.; Bryden, T.; Jones, T. S.; Beeby, A.; Samuel, I. D. W. *Synth. Met.* **2003**, *138*, 463. (e) Dickins, R. S.; Aime, S.; Batsanov, A. S.; Beeby, A.; Botta, M.; Bruce, J.; Howard, J. A. K.; Love, C. S.; Parker, D.; Peacock, R. D.; Buschmann, H. *J. Am. Chem. Soc.* **2002**, *124*, 12697. (f) Wong, W. K.; Liang, H. Z.; Wong, W. Y.; Cai, Z. W.; Li, K. F.; Cheah, K. W. *New J. Chem.* **2002**, *26*, 275. (g) Silva, F. R. G. E.; Malta, O. L.; Reinhard, C.; Güdel, H. U.; Piguet, C.; Moser, J. E.; Bunzli, J.-C. G. *J. Phys. Chem. A* **2002**, *106*, 1670. (h) Faulkner, S.; Beeby, A.; Carrie, M. C.; Dadabhoy, A.; Kenwright, A. M.; Sammes, P. G. *Inorg. Chem. Commun.* **2001**, *4*, 187. (i) Hebbink, G. A.; Klink, S. I.; Oude Alink, P. G. B.; van Veggel, F. C. J. M. *Inorg. Chim. Acta* **2001**, *317*, 114. (j) Voloshin, A. I.; Shavaleev, N. M.; Kazakov, V. P. *J. Lumin.* **2001**, *93*, 199. (k) Driesen, K.; Nockemann, P.; Binnemans, K. *Chem. Phys. Lett.* **2004**, *395*, 306. (l) Bassett, A. P.; Magennis, S. W.; Glover, P. B.; Lewis, D. J.; Spencer, N.; Parsons, S.; Williams, R. M.; De Cola, L.; Pikramenou, Z. *J. Am. Chem. Soc.* **2004**, *126*, 9413. (m) Driesen, K.; Van Deun, R.; Gorller-Walrand, C.; Binnemans, K. *Chem. Mater.* **2004**, *16*, 1531.

(3) Klink, S. I.; Keizer, H.; van Veggel, F. C. J. M. *Angew. Chem., Int. Ed.* **2000**, *39*, 4319.

(4) (a) Beeby, A.; Dickins, R. S.; FitzGerald, S.; Govenlock, L. J.; Maupin, C. L.; Parker, D.; Riehl, J. P.; Siligardi, G.; Williams, J. A. G. *Chem. Commun.* **2000**, 1183. (b) Imbert, D.; Cantuel, M.; Bünzli, J.-C. G.; Bernardinelli, G.; Piguet, C. *J. Am. Chem. Soc.* **2003**, *125*, 15698. (c) Pope, S. J. A.; Coe, B. J.; Faulkner, S. *Chem. Commun.* **2004**, 1550. (d) Pope, S. J. A.; Coe, B. J.; Faulkner, S.; Bichenkova, E. V.; Yu, X.; Douglas, K. T. *J. Am. Chem. Soc.* **2004**, *126*, 9490. (e) Guo, D.; Duan, C.-Y.; Lu, F.; Hasegawa, Y.; Meng, Q.-J.; Yanagida, S. *Chem. Commun.* **2004**, 1486. (f) Glover, P. B.; Ashton, P. R.; Childs, L. J.; Rodger, A.; Kercher, M.; Williams, R. M.; De Cola, L.; Pikramenou, Z. *J. Am. Chem. Soc.* **2003**, *125*, 9918.

(5) (a) Shavaleev, N. M.; Bell, Z. R.; Ward, M. D. *J. Chem. Soc., Dalton Trans.* **2002**, 3925. (b) Shavaleev, N. M.; Moorcraft, L. P.; Pope, S. J. A.; Bell, Z. R.; Faulkner, S.; Ward, M. D. *Chem. Commun.* **2003**, 1134. (c) Shavaleev, N. M.; Moorcraft, L. P.; Pope, S. J. A.; Bell, Z, R.; Faulkner, S.; Ward, M. D. *Chem.—Eur. J.* **2003**, *9*, 5283. (d) Shavaleev, N. M.; Accorsi, G.; Virgili, D.; Bell, Z. R.; Lazarides, T.; Calogero, G.; Armaroli, N.; Ward, M. D. *Inorg. Chem.* **2005**, in press.

(6) (a) Timpson, C. J.; Bignozzi, C. A.; Sullivan, B. P.; Kober, E. M.; Meyer, T. J. *J. Phys. Chem.* **1996**, *100*, 2915.

(7) (a) Liu, S.; Meyers, E. A.; Shore, S. G. *Angew. Chem., Int. Ed.* **2002**, *41*, 3609. (b) Plecnik, C. E.; Liu, S.; Shore, S. G. *Acc. Chem. Res.* **2003**, *36*, 499 and refs therein.

(8) (a) Rawashdeh-Omary, M. A.; Larochelle, C. L.; Patterson, H. H. *Inorg. Chem.* **2000**, *39*, 4527. (b) Assefa, Z.; Shankle, G.; Patterson, H. H.; Reynolds, R. *Inorg. Chem.* **1994**, *33*, 2187.

(9) (a) Ma, B.-Q.; Gao, S.; Su, G.; Xu, G.-X. *Angew. Chem., Int. Ed.* **2001**, *40*, 434. (b) Figuerola, A.; Diaz, C.; Ribas, J.; Tangoulis, V.; Granell, J.; Lloret, F.; Mahia, J.; Maestro, M. *Inorg. Chem.* **2003**, *42*, 641. (c) Toma, L. M.; Delgado, F. S.; Ruiz-Pérez, C.; Carrasco, R.; Cano, J.; Lloret, F.; Julve, M. *Dalton Trans.* **2004**, 2836. (d) Herrera, J. M.; Marvaud, V.; Verdaguer, M.; Marrot, J.; Kalisz, M.; Mathonière, C. *Angew. Chem., Int. Ed.* **2004**, *43*, 5468.

(10) (a) Goubard, F.; Tabuteau, A. *Struct. Chem.* **2003**, *14*, 257. (b) Mullica, D. F.; Farmer, J. M.; Cunningham, B. P.; Kautz, J. A. *J. Coord. Chem.* **2000**, *49*, 239. (c) Kautz, J. A.; Mullica, D. F.; Cunningham, B. P.; Coombs, R. A.; Farmer, J. M. *J. Mol. Struct.* **2000**, *523*, 175. (d) Mullica, D. F.; Farmer, J. M.; Kautz, J. A. *Inorg. Chem. Commun.* **1999**, *2*, 73. (e) Miller, T. A.; Jeffery, J. C.; Ward, M. D. *CrystEngComm* **2003**, *5*, 495.

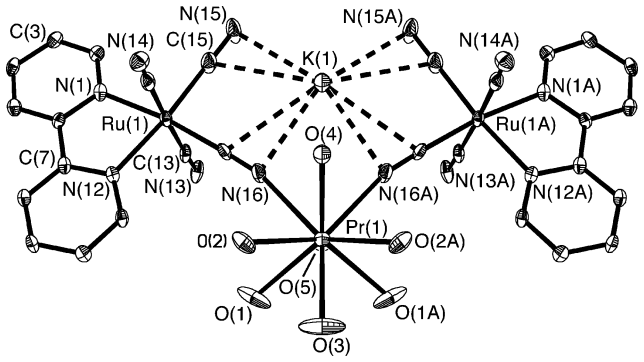


**Figure 1.** Molecular structure of **$Ru_2PrK$** showing thermal ellipsoids at the 40% probability level. Disordered water ligands attached to K(1) are not shown.

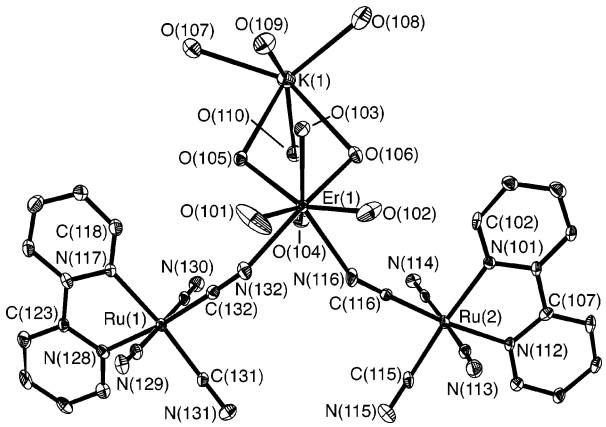


**Figure 2.** Structure of one of the independent complex units of **$Ru_2ErK$** showing thermal ellipsoids at the 40% probability level.

## Results and Discussion

**Syntheses and Structures.** Slow evaporation of aqueous solutions containing a mixture of $K_2[Ru(bipy)(CN)_4]$ and a lanthanide(III) chloride (Ln = Pr, Nd, Gd, Er, Yb) afforded, in varying yields, crops of crystalline products. Their IR spectra all showed two cyanide stretching vibrations, one in the 2038−2050 $cm^{-1}$ region (consisting of several overlapping components), and a second just above 2100 $cm^{-1}$. The structural determinations described below showed that the materials fall into one of two structural types. These are (a) $[\{Ru(bipy)(CN)_4\}_2\{Ln(H_2O)_m\}\{K(H_2O)_n\}]\cdot xH_2O$ (Ln = Pr, Er, Yb; $m$ = 7, 6, 6, respectively), in which one $Ln^{3+}$ ion and one $K^+$ ion balance the charge of two $[Ru(bipy)(CN)_4]^{2-}$ units, and (b) $[\{Ru(bipy)(CN)_4\}_3\{Ln(H_2O)_4\}_2]\cdot xH_2O$ (Ln = Nd, Gd), in which no $K^+$ ions are required because three $[Ru(bipy)(CN)_4]^{2-}$ units are charge-balanced by two $Ln^{3+}$ ions. In all cases, there are numerous additional lattice water molecules, as shown in the crystal structures and also reflected in the elemental analyses. For the sake of simplicity, we abbreviate the former series as **$Ru_2LnK$** (Ln = Pr, Er, Yb) and the latter series as **$Ru_3Ln_2$** (Ln = Nd, Gd).

The structure of **$Ru_2PrK$** is shown in Figure 1. The structure contains tetranuclear $Ru_2PrK$ units, in which two $[Ru(bipy)(CN)_4]^{2-}$ units are linked to a $\{Pr(H_2O)_7\}^{3+}$ fragment by one cyanide bridge each; the Pr(III) center is, therefore, nine-coordinate with a capped square antiprismatic geometry [the square planes are O(3)/O(4)/O(2)/O(2A) and N(16)/N(16A)/O(1)/O(1A), with O(5) being the cap]. The cluster has 2-fold symmetry with K(1), Pr(1), O(3), O(4), and O(5) lying on a mirror plane. The $K^+$ cation is in a rather unusual coordination environment, in a pocket delineated by four cyanide groups, C(15)/N(15) and C(16)/N(16), and their two symmetry equivalents; these eight C and N atoms are essentially coplanar. The $K^+$ cation is coordinated by these four cyanides in a side-on manner reminiscent of alkyne $\pi$ bonding, with the K−C separations (average 3.22 Å) somewhat longer than the K−N interactions (average 3.05 Å); it lies only slightly (0.025 Å) out of the mean plane of the eight C and N donor atoms. This type of bonding of cyanides to alkali metal ions has recently been observed by Rauchfuss et al. in numerous cyanometalate cages, where bridging cyanides along the edges of a cage are also interacting in a side-on manner with an alkali metal cation trapped in the center of the cavity.[12] Gokel and co-workers have demonstrated similar side-on interactions between alkene/alkyne units and alkali metal cations.[13] In **$Ru_2PrK$**, the K−C and K−N separations are comparable to those observed in the few other examples of $K^+$ cyanide[12b] or alkyne[13d] complexes of this type.

Of the four side-on binding cyanide groups, two [C(16)/N(16) and the symmetry equivalent] are also involved in a more conventional end-on coordination of the cyanide ligand to the Pr center [C(16)−N(16)−Pr(1) angle, 166.7°]. The Ru···Pr separation is 5.627 Å. The $K^+$ cation also has two water ligands, one above and one below the approximate $KC_4N_4$ plane; these are each disordered over two sites. One of these, O(6), is involved in a hydrogen-bonding interaction with O(4) (coordinated to the Pr center): the nonbonded separation O(4)···O(6) [and likewise, O(4)···O(6A)] is 2.82 Å. In addition, there are 10 lattice water molecules associated with each **$Ru_2PrK$** unit. These are involved in hydrogen-bonding interactions with each other, with the water ligands attached to Pr(1) and K(1) and also with the "free" cyanide N atoms N(13) and N(14), as shown by numerous nonbonded O···O and O···N contacts of < 3 Å. Examination of a packing diagram shows that the discrete **$Ru_2PrK$** units are associated in the crystal by intercluster hydrogen bonds involving several of the water ligands on Pr(1) and K(1).

The structure of **$Ru_2ErK$** is shown in Figures 2 and 3 and is basically similar to that of **$Ru_2PrK$**, albeit with some significant differences. There are two complete and independent tetranuclear **$Ru_2ErK$** clusters in the asymmetric unit, of which only one is shown in the figures; the other is very similar. Again, two $[Ru(bipy)(CN)_4]^{2-}$ units are linked to the lanthanide fragment by one cyanide bridge each, but the $Er^{3+}$ ions have six additional water ligands, rather than seven

(11) Miller, T. A.; Jeffery, J. C.; Ward, M. D.; Adams, H.; Pope, S. J. A.; Faulkner, S. *Dalton Trans.* **2004**, 1524.

(12) (a) Contakes, S. M.; Rauchfuss, T. B. *Chem. Commun.* **2001**, 553. (b) Contakes, S. M.; Rauchfuss, T. B. *Angew. Chem., Int. Ed.* **2000**, *39*, 1984. (c) Kuhlman, M. L.; Rauchfuss, T. B. *J. Am. Chem. Soc.* **2003**, *125*, 10084.

(13) (a) Hu, J. X.; Barbour, L. J.; Gokel, G. W. *Collect. Czech. Chem. Commun.* **2004**, *69*, 1050. (b) Hu, J.; Gokel, G. W. *Chem. Commun.* **2003**, 2537. (c) Gokel, G. W. *Chem. Commun.* **2003**, 2847. (d) Hu, J.; Barbour, L. J.; Gokel, G. W. *J. Am. Chem. Soc.* **2001**, *123*, 9486.

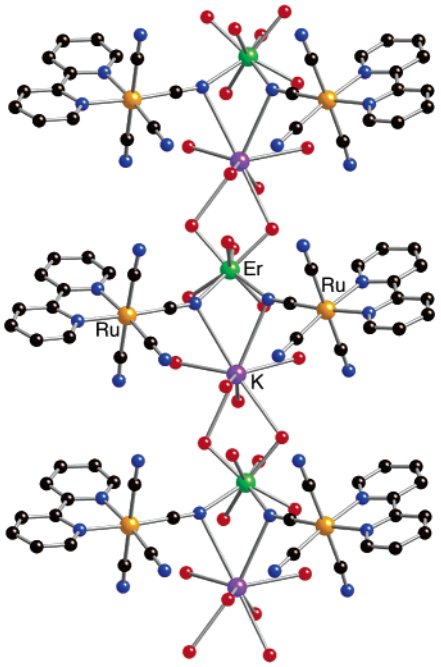


**Figure 3.** Chain structure of **$Ru_2ErK$**.

(as seen for Pr, above), an effect arising from the smaller ionic radius of $Er^{3+}$ compared to that of $Pr^{3+}$. The $Er^{3+}$ center is, therefore, eight-coordinate and approximately a square antiprism, with N(132), N(116), O(101), and O(102) describing one plane and O(103), O(104), O(105), and O(106) describing the other. The Ru(1)···Er(1) and Ru(2)···Er(1) separations are 5.442 and 5.352 Å, respectively.

The main difference between this structure and that of **$Ru_2PrK$** is that the $K^+$ ions are disposed differently. In Figures 2 and 3, we see that the $K^+$ ion is no longer interacting with a near-planar array of four cyanide groups; instead, it is coordinated by water molecules. Four of these [O(107), O(108), O(109), O(110)] are terminal and have K−O separations in the range 2.8−2.9 Å. O(105) and O(106), however, are bridging water molecules shared with Er(1), as a result of which, these K−O separations are longer than the others (3.03 and 3.22 Å, respectively). The packing diagram (Figure 3) reveals two long-distance interactions with the N atoms of cyanide ligands [N(116) and N(132) of the neighboring **$Ru_2ErK$** unit; these K···N distances are 3.36 and 3.34 Å, respectively]. There is no evidence for any interaction with the $\pi$ electrons of these cyanide ligands, as the K···C distances to the C atoms of these cyanide units are > 3.8 Å and the geometry is clearly not "side-on". Consequently, the tetranuclear **$Ru_2ErK$** units are associated into a columnar stack via a weak interaction of the $K^+$ ion of one unit with the bridging Ru−CN−Er cyanide ligands of the next one. Although the K···N separations are rather long, the displacement of the N atoms toward the $K^+$ ions results in nonlinear coordination of these cyanide ligands to the Er(III) ions, with C−N−Er angles in the range 150−160°. These cyanide ligands, therefore, interact with all three metal ions in the lattice and are responsible for both the Ru−CN−Er interactions and the longer-range interactions with $K^+$ that link the **$Ru_2ErK$** units. The $K^+$ ions can, therefore, be considered as eight-coordinate, with four terminal water ligands, two bridging water ligands (to Er in one direction), and two bridging cyanide ligands (to Er in the other direction).

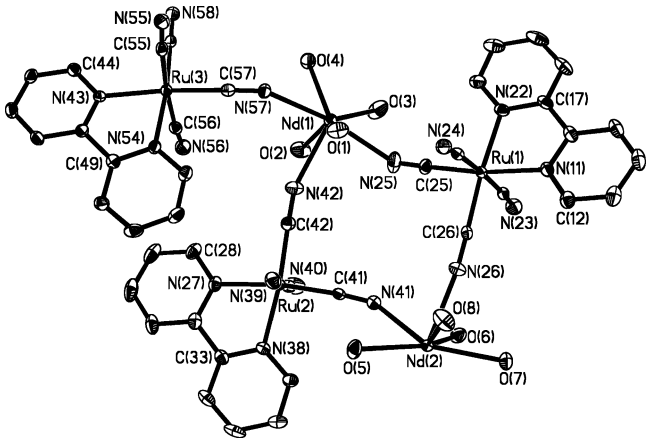


**Figure 4.** Asymmetric unit of the crystal structure of **$Ru_3Nd_2$** showing thermal ellipsoids at the 40% probability level.

The crystallographically independent unit containing Ru(3), Ru(3), Er(2), and K(2) is structurally very similar, and all of the comments above apply equally to the geometry of the **$Ru_2ErK$** unit and to the packing; the Ru(3)···Er(2) and Ru(4)···Er(2) separations are 5.345 and 5.439 Å, respectively. The lattice also contains 10 water molecules in the asymmetric unit (five water molecules *per* tetranuclear **$Ru_2ErK$** unit), which are involved in hydrogen-bonding interactions with each other, the coordinated water molecules on the $Er^{3+}$ centers, and the external lone pairs of some of the cyanide ligands, as shown by numerous O···O and O···N contacts involving lattice water molecules in the range 2.6−3 Å.

**$Ru_2YbK$** is isostructural and isomorphous with **$Ru_2ErK$**, and its structure was discussed in an earlier communication,[11] so it is not necessary to repeat it here. The Ru···Yb separations are in the range 5.32−5.44 Å.

**$Ru_3Nd_2$** and **$Ru_3Gd_2$** are isostructural and isomorphous. The asymmetric unit of **$Ru_3Nd_2$** is shown in Figure 4; there are three crystallographically unique $[Ru(bipy)(CN)_4]^{2-}$ units and two $Nd^{3+}$ centers. Ru(1), Ru(2), Nd(1), and Nd(2) form the corners of an approximate square with Ru−CN−Nd cyanide bridges along each edge. Figures 5 and 6 show how the structure propagates to form a complicated two-dimensional polymeric network. The main repeating unit in the structure is the set of five fused rings shown in Figure 5. Of these, rings 1, 3, and 5 in the sequence (like the ring shown in Figure 4) may be described as approximately square, whereas rings 2 and 4 are more obviously buckled with the four metal atoms forming a butterfly shape. These propagate into a two-dimensional array by the sharing of Gd "corners" between adjacent five-ring units. Figure 6 shows a view looking edge-on at the cyanide-bridged sheet and illustrates how each sheet is capped above and below by bipyridyl ligands. Nd(1) is eight-coordinate, with four water and four cyanide ligands; with reference to the view in Figure 4, the coordination sphere is completed by N(55)

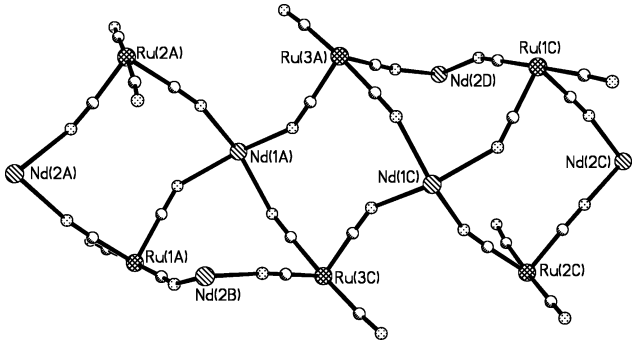


**Figure 5.** Part of the two-dimensional sheet structure in $\mathbf{Ru_3Nd_2}$, showing only the metal ions and the cyanide bridging ligands.

from a cyanide ligand in an adjacent asymmetric unit. Nd(2) likewise has four water and four cyanide ligands, with the coordination sphere, as shown in Figure 4, being completed by N(24) and N(58) from adjacent asymmetric units. The $[Ru(bipy)(CN)_4]^{2-}$ units containing Ru(1), Ru(2), and Ru(3) are involved in two, three, and three Ru−CN−Nd bridging interactions to $Nd^{3+}$ centers, respectively. Thus, the three Ru units provide a total of eight cyanide donors to $Nd^{3+}$, and each of the two $Nd^{3+}$ centers accepts four of these. The Ru···Nd separations lie in the range 5.35−5.63 Å (for $\mathbf{Ru_3Gd_2}$, the Ru···Gd separations are in the range 5.27−5.59 Å). There are 11 lattice water molecules in each asymmetric unit (some disordered over two sites), which, as usual, form networks of hydrogen bonds with each other, with water ligands on the $Nd^{3+}$ centers and free N lone pairs from those cyanide ligands that are not involved in coordination to the $Nd^{3+}$ ions.

**Photophysical Properties.** From the point of view of investigating Ru → Ln energy transfers, the presence of different structural types among the compounds prepared is expected to be of little significance. Both Förster and Dexter energy transfers are strongly distance-dependent ($r^{-6}$ and $e^{-r}$, respectively), so energy-transfer rates will be dominated by the shortest Ru···Ln contact whatever the bulk structure. If Dexter energy transfer is occurring, exploiting the through-bond Ru−CN−Ln electronic coupling, then more remote lanthanide centers will not significantly contribute to the quenching of a particular Ru center.

The photophysical properties of the $[Ru(bipy)(CN)_4]^{2-}$ energy-donor unit are known to be strongly environment-dependent.[14] The interaction of the externally directed lone pairs of the cyanide ligands with hydrogen-bond donors such as protic solvent molecules or ammonium cations increases the ligand field strength at the metal center and results in a higher energy and longer-lived $^3$MLCT state compared to the case where such interactions are absent. Thus, the luminescence lifetimes in different solvents can vary from a few nanoseconds to about a microsecond. As the control for our Ru−lanthanide systems we used the Ru/Gd complex $\mathbf{Ru_3Gd_2}$. The lowest excited state of Gd(III) lies > 30 000 $cm^{-1}$ above the ground state and, consequently, cannot act as an energy acceptor in these complexes; however, the presence of $Gd^{3+}$ cations attached to some of the cyanide lone pairs will have a significant electrostatic effect on the energy of the $[Ru(bipy)(CN)_4]^{2-}$ $^3$MLCT state, which needs to be taken into account. Solid-state luminescence measurements on $\mathbf{Ru_3Gd_2}$ showed the characteristic strong luminescence from the $^3$MLCT state of $[Ru(bipy)(CN)_4]^{2-}$ at 580 nm. The effect of the $Gd^{3+}$ cations on the luminescence of the $[Ru(bipy)(CN)_4]^{2-}$ is clear; in water, the luminescence occurs at about 640 nm,[14] and in solid $K_2[Ru(bipy)(CN)_4]$, this blue-shifts substantially to 584 nm.[11] The emission maximum of 580 nm for $\mathbf{Ru_3Gd_2}$ is comparable to that of the $K^+$ salt, for the same reasons: coordination of the cyanide lone pairs to an electropositive metal ion will increase the ability of the C terminus of the cyanide to act as a $\pi$ acceptor, thereby increasing the ligand field strength at the Ru(II) center and increasing the $^3$MLCT energy.

Time-resolved measurements of the Ru-based emission in $\mathbf{Ru_3Gd_2}$ illustrate the particular problems of performing luminescence measurements with solids rather than solutions. In the crystal structure of $\mathbf{Ru_3Gd_2}$, there are three crystallographically independent Ru centers, all with slightly different second-sphere coordination environments. In particular, one of the Ru centers only has two Ru−CN−Gd bridges, whereas the other two have three. Given that the luminescence behavior of the $[Ru(bipy)(CN)_4]^{2-}$ unit is unusually sensitive to second-sphere effects, as described above, it follows that we do not expect to see the simple single-exponential luminescence decay that is normally observed in solution. In addition, the presence of defect sites in the crystal, and surface effects (whereby luminescent centers on the surface of a particle are in a different environment from those in the bulk), can complicate matters further. The Ru-based luminescence decay of $\mathbf{Ru_3Gd_2}$ could, however, be fitted approximately to a single-exponential decay with $\tau = 550$ ns. For comparison, luminescence from solid (hydrated) $K_2[Ru(bipy)(CN)_4]$ could be fitted to a dual-exponential decay with lifetimes of 750 and 2950 ns.[11] The presence of $Gd^{3+}$ ions in $\mathbf{Ru_3Gd_2}$, therefore, has a slight quenching effect on the Ru-based luminescence compared to $K^+$ ions.

For all other complexes, to maximize the sensitized lanthanide emission, which is inherently weak in the NIR region, crystals for photophysical analysis were grown from $D_2O$ rather than from $H_2O$. This will minimize the quenching associated with OH oscillators close to the lanthanide. The quenching effect of OH oscillators is particularly severe for the NIR-luminescent lanthanides because the low energy of the excited states involved means that a lower excited state of the OH oscillator is needed for accepting the energy, compared to the situation with, for example, $Tb^{3+}$ and $Eu^{3+}$, thereby making quenching more likely.[5c,15] In every case, excitation at 337 nm into the absorption manifold of the $[Ru(bipy)(CN)_4]^{2-}$ unit resulted in the appearance of sensi-

(14) (a) Timpson, C. J.; Bignozzi, C. A.; Sullivan, B. P.; Kober, E. M.; Meyer, T. J. *J. Phys. Chem.* **1996**, *100*, 2915. (b) Simpson, N. R. M.; Ward, M. D.; Morales, A. F.; Ventura, B.; Barigelletti, F. *J. Chem. Soc., Dalton Trans.* **2002**, 2455. (c) Simpson, N. R. M.; Ward, M. D.; Morales, A. F.; Barigelletti, F. *J. Chem. Soc., Dalton Trans.* **2002**, 2449. (d) Rampi, M. A.; Indelli, M. T.; Scandola, F.; Pina, F.; Parola, A. J. *Inorg. Chem.* **1996**, *35*, 3355. (e) Borsarelli, C. D.; Braslavsky, S. E.; Indelli, M. T.; Scandola, F. *Chem. Phys. Lett.* **2000**, *317*, 53. (f) Kovács, M.; Horváth, A. *Inorg. Chim. Acta* **2002**, *335*, 69.

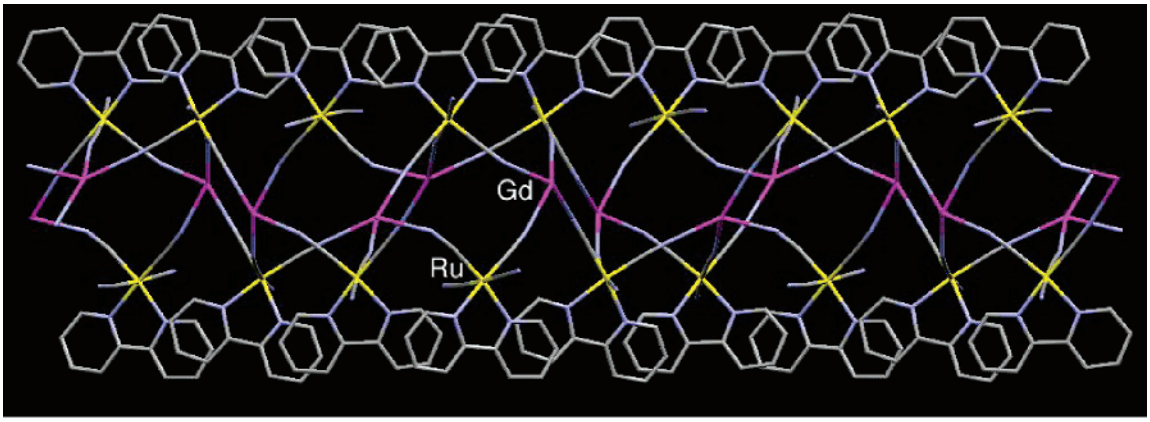


**Figure 6.** View of **$Ru_3Nd_2$** looking edge-on at the two-dimensional sheets, showing the capping arrangement of bipy ligands above and below the sheets.

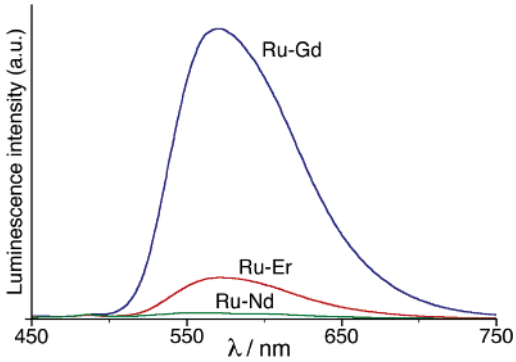


**Figure 7.** Ru-based luminescence from three of the coordination networks showing the variation in intensity produced by different degrees of quenching by the lanthanide.

tized NIR luminescence characteristic of the lanthanide present (980 nm for Yb, 840 and 1010 nm for Pr, 1530 nm for Er, and 1055 and 1340 nm for Nd). In addition, there was, in every case, residual luminescence centered at 570−580 nm arising from the $[Ru(bipy)(CN)_4]^{2-}$ centers that are not completely quenched (Figure 7). The intensity of the Ru-based luminescence in every case is, however, much less than that in **$Ru_3Gd_2$** as a consequence of the energy transfer to the lanthanide, with Yb affording the smallest degree of quenching (still a quite strong Ru-based emission) and Nd the greatest (only a very weak Ru-based emission). On this basis, the degree of quenching of the Ru-based luminescence, and hence the efficiency of the energy transfer to the lanthanide, follows the order Nd > Pr > Er > Yb > Gd.

Time-resolved measurements on the Ru-based emission (measured at 700 nm) were in agreement with this behavior. In three cases (**$Ru_2ErK$**, **$Ru_2PrK$**, and **$Ru_3Nd_2$**), the Ru-based emission could be fitted better to a dual exponential decay than to a single one, with the short-lived component dominating and a small amount of a long-lived component also present. The $\tau$ values, and the pre-exponential $A$ values (which determine the relative weighting of the two components), are given in Table 1. In these three cases, the minor long-lived component, which has a weighting of <5% compared to that of the short-lived component, has a lifetime in the 300−500 ns region, which corresponds approximately to the "unquenched" lifetime obtained for the Ru-based emission **$Ru_3Gd_2$** in the absence of an energy transfer. We therefore ascribe this minor long-lived luminescence component to a small proportion of $[Ru(bipy)(CN)_4]^{2-}$ units that are not connected to a lanthanide center because of defect sites in the crystal or surface effects (the crystals are ground into powders for photophysical analysis). In the case of **$Ru_2YbK$**, the luminescence at 700 nm fitted reasonably well to a single-exponential decay corresponding to the partially quenched Ru centers.

**Table 1.** Luminescence Data

| complex | Ru-based emission $\tau$, ns[a] | Ln-based emission $\tau$, ns | Ru → Ln energy-transfer rate[b] $k_{EnT}$, $s^{-1}$ |
|---|---|---|---|
| **$Ru_3Gd_2$** | 550 | | |
| **$Ru_2YbK$** | 197 | 197[c] | $3 \times 10^6$ [d] |
| **$Ru_2ErK$** | 76 | *e* | $1 \times 10^7$ |
| | 437 (4%) | | |
| **$Ru_2PrK$** | 22 | 22[f] | $4 \times 10^7$ |
| | 273 (3%) | | |
| **$Ru_3Nd_2$** | 5 | 45[g] | $2 \times 10^8$ |
| | 439 (<1%) | | |

[a] Measured at 700 nm. For the lower three entries, the Ru-based luminescence has a weak longer-lived component, which is the second entry; the pre-exponential value (relative to the main component taken as 100%) is given as a percentage in parentheses. [b] Determined using eq 1 (see main text). [c] Measured at 980 nm; the Yb-based luminescence overlaps with the tail of the Ru-based luminescence, and the two components cannot be separated. This value will, therefore, be subject to a large error. [d] The rise time of the 980 nm emission gives an alternative estimate of $6 \times 10^6$ $s^{-1}$ (see main text). [e] Luminescence too weak to get a meaningful value for the lifetime. [f] Measured at 1010 nm. [g] Measured at 1055 nm.

Taking the major (>95% on the basis of the pre-exponential factors) luminescence component as arising from residual $[Ru(bipy)(CN)_4]^{2-}$ luminescence following an energy transfer across the Ru−CN−Ln bridge, we can use eq 1 to estimate the rate of energy transfer $k_{EnT}$; $\tau_q$ is the residual Ru-based lifetime in the presence of quenching, and $\tau$ is the unquenched lifetime, in this case, taken from **$Ru_3Gd_2$**. In the cases where $\tau_q \ll \tau$, the value of $1/\tau$ becomes relatively insignificant and eq 1 reduces to $k_{EnT} \approx 1/\tau_q$.

$$k_{EnT} = 1/\tau_q - 1/\tau \qquad (1)$$

From eq 1 (and taking $\tau$ = 550 ns for the unquenched luminescence of **$Ru_3Gd_2$**, see above), we can derive Ru →

(15) Beeby, A.; Clarkson, I. M.; Dickins, R. A.; Faulkner, S.; Parker, D.; Royle, L.; de Sousa, A. S.; Williams, J. A. G.; Woods, M. *J. Chem. Soc., Perkin Trans. 2* **1999**, 493.

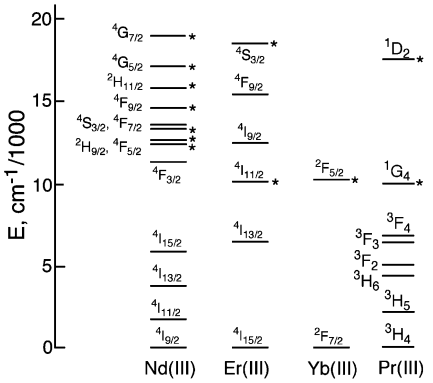


**Figure 8.** Relevant lanthanide-based energy levels; those marked with * can act as energy acceptors by either Förster or Dexter mechanisms and are of an appropriate energy to overlap with the Ru-based emission (between 10 000 $cm^{-1}$ and 19 000 $cm^{-1}$; see text).

lanthanide energy-transfer rates of $2 \times 10^8$ $s^{-1}$ for $Nd^{3+}$, $4 \times 10^7$ $s^{-1}$ for $Pr^{3+}$, $1 \times 10^7$ $s^{-1}$ for $Er^{3+}$, and $3 \times 10^6$ $s^{-1}$ for $Yb^{3+}$, in agreement with the relative intensities of the residual Ru-based luminescences. Given the particular problems associated with solid-state measurements, as described earlier, the uncertainties on these values will be higher than would occur from solution-based measurements and the energy-transfer rates are given to one significant figure only. However, they cover a sufficiently large spread (2 orders of magnitude), with at least a factor of 3 between each member of the series, for the ordering to be unambiguous.

There are few examples of d−f systems in which energy-transfer rates have been quantified. The values derived here may be compared with the much lower values of $k_{EnT} < 10^5$ $sec^{-1}$ for a $[Ru(bipy)_3]^{2+}/Yb^{3+}$ dyad and $k_{EnT} = 1.1 \times 10^6$ $sec^{-1}$ for a $[Ru(bipy)_3]^{2+}/Nd^{3+}$ dyad, described by van Veggel and co-workers.[3] The much lower energy-transfer rates in those systems compared to ours reflect the greater metal−metal separations and the absence of a directly conjugated bridging pathway.

The large variation in energy-transfer rates that we have observed, spanning 2 orders of magnitude, can be accounted for by differences in the overlap between the emission spectrum of the donor (Ru) component and the absorption spectrum of the acceptor (lanthanide) component. The Ru···Ln distances span a very narrow range, and minor variations in this parameter will make only a small contribution to the energy transfer; in fact, the complex with the shortest Ru···Ln separation is **$Ru_2YbK$**, which has the slowest energy transfer. Figure 8 shows the electronic energy levels for the lanthanide ions concerned. The high-energy end of the Ru-based emission is at 500 nm (20 000 $cm^{-1}$), so we can take this as the $^3$MLCT energy and ignore any higher-lying lanthanide energy levels. A gradient of at least 1000 $cm^{-1}$ for an energy transfer from an excited triplet donor to a lanthanide will be necessary to prevent a thermally activated back energy transfer at room temperature,[16] so no lanthanide energy levels above 19 000 $cm^{-1}$ are likely to play a role in quenching the Ru-based luminescence. At the low-energy end of the spectrum, the Ru-based emission has decayed to almost nothing by about 1000 nm (10 000 $cm^{-1}$; see, e.g., Figures 7 and 9), so we can ignore any lower-lying lanthanide levels as having insignificant spectral overlap with the energy donor.

$Yb^{3+}$ has only a single f−f transition at about 10 200 $cm^{-1}$, which just overlaps with the low-energy tail of the Ru-based emission,[11] and it is clear that the overlap, although nonzero, will be small compared to all of the other cases described here. In contrast, $Nd^{3+}$ has a particularly high density of energy levels between ca.10 000 and 20 000 $cm^{-1}$, with many of them lying in the region where the Ru-based emission is at its most intense (above 15 000 $cm^{-1}$), so it is clear why the Ru → Nd energy transfer should be the most efficient. $Er^{3+}$ has six energy levels in the relevant range, from $^4I_{11/2}$ up to $^4I_{7/2}$, available to act as energy acceptors (more than $Yb^{3+}$ but fewer than $Nd^{3+}$). As we have seen, $Er^{3+}$ gives an intermediate level of quenching consistent with this. For $Pr^{3+}$, only $^1D_2$ and $^1G_4$ are of the correct energy, but the former of these, at about 17 500 $cm^{-1}$, perfectly matches the maximum of the Ru-based emission.

It is also necessary to take into account the selection rules for energy transfers. There are separate selection rules for Förster and Dexter energy transfers, with the former requiring $|\Delta J| = 2$, 4, or 6 at the lanthanide and the latter requiring $|\Delta J| = 0$ or 1 (with the exception of $J = J' = 0$, which is forbidden).[17] In Figure 8, those energy levels that can act as energy acceptors according to either of these selection rules, and which also lie between 10 000 and 19 000 $cm^{-1}$ above the ground state, are shown with an asterisk (*). It will be apparent that most of the $Nd^{3+}$ energy levels that overlap with the Ru-based emission remain available for quenching in **$Ru_3Nd_2$**, and it is clear why the Ru → Nd energy transfer should be the fastest. An energy transfer to the single excited state of $Yb^{3+}$ in **$Ru_2YbK$** is likewise allowed, by the Dexter mechanism, but the very poor spectral overlap means that the Ru → Yb energy transfer is expected to be relatively slow. For $Er^{3+}$, the $^4F_{9/2}$ and $^4I_{9/2}$ levels, which would contribute significantly to the spectral overlap with the Ru emission, are forbidden from participating. The $^4I_{11/2}$ level at ca.10 000 $cm^{-1}$ will give only very little overlap with the tail of the Ru-based emission; the next highest level that is allowed to be an energy acceptor is $^4S_{3/2}$ at ca. 18 300 $cm^{-1}$, which overlaps with the high-energy end of the Ru-based emission and may, therefore, play a significant role in quenching, although an energy transfer to this level is only slightly endergonic (<2000 $cm^{-1}$) and may, therefore, be inefficient because of a thermally activated back energy transfer to the Ru-based $^3$MLCT level. The $Er^{3+}$ levels above this are likely to be too high in energy to participate. $Pr^{3+}$ has only two levels of the appropriate energy, but an energy transfer to both is allowed. The position of the $^1D_2$ level, overlapping with the Ru emission maximum, suggests an

(16) (a) Sabbatini, N.; Guardigli, M.; Lehn, J.-M. *Coord. Chem. Rev.* **1993**, *123*, 201. (b) Armaroli, N.; Accorsi, G.; Barigelletti, F.; Couchman, S. M.; Fleming, J. S.; Harden, N. C.; Jeffery, J. C.; Mann, K. L. V.; McCleverty, J. A.; Rees, L. H.; Starling, S. R.; Ward, M. D. *Inorg. Chem.* **1999**, *38*, 5769.

(17) de Sá, G. F.; Malta, O. L.; de Mello Donegá, C.; Simas, A. M.; Longo, R. L.; Santa-Cruz, P. A.; da Silva, E. F. *Coord. Chem. Rev.* **2000**, *196*, 165.

**Table 2.** Summary of Crystal, Data Collection, and Refinement Details

| complex | $[\{Ru(bipy)(CN)_4\}_2\{Pr(H_2O)_7\}\{K(H_2O)_2\}]\cdot 10H_2O$ | $[\{Ru(bipy)(CN)_4\}_2\{Er(H_2O)_6\}\{K(H_2O)_4\}]\cdot 5H_2O$ |
|---|---|---|
| formula | $C_{28}H_{54}KN_{12}O_{19}PrRu_2$ | $C_{28}H_{46}ErKN_{12}O_{15}Ru_2$ |
| molecular weight | 1244.98 | 1199.27 |
| cryst syst | monoclinic | tetragonal |
| space group | $P2_1/m$ | $Pca2_1$ |
| *a*, Å | 9.006(2) | 17.226(3) |
| *b*, Å | 29.787(7) | 29.365(2) |
| *c*, Å | 9.505(2) | 17.226(3) |
| α, deg | 90 | 90 |
| *β*, deg | 115.048(4) | 90 |
| *γ*, deg | 90 | 90 |
| *V*, Å$^3$ | 2310.0(1.0) | 8713.9(9) |
| *Z* | 2 | 8 |
| *ρ*, g cm$^{-3}$ | 1.790 | 1.828 |
| cryst size, mm$^3$ | 0.37 × 0.33 × 0.23 | 0.40 × 0.40 × 0.42 |
| *μ*, mm$^{-1}$ | 1.856 | 2.764 |
| data, restraints, params | 5376, 0, 281 | 19724, 1, 1064 |
| final R1, wR2 | 0.0593, 0.1869 | 0.0393, 0.1063 |

| complex | $[\{Ru(bipy)(CN)_4\}_3\{Nd(H_2O)_4\}_2]\cdot 11H_2O$ | $[\{Ru(bipy)(CN)_4\}_3\{Gd(H_2O)_4\}_2]\cdot 11H_2O$ |
|---|---|---|
| formula | $C_{42}H_{24}N_{18}Nd_2O_{19}Ru_3$ | $C_{42}H_{24}Gd_2N_{18}O_{19}Ru_3$ |
| molecular weight | 1676.48 | 1722.66 |
| cryst syst | monoclinic | monoclinic |
| space group | $P2_1/c$ | $P2_1/c$ |
| *a*, Å | 15.0504(14) | 14.9452(11) |
| *b*, Å | 13.7872(13) | 13.7769(10) |
| *c*, Å | 29.790(3) | 29.611(2) |
| α,° | 90 | 90 |
| *β*,° | 104.599(2) | 104.3020(10) |
| *γ*,° | 90 | 90 |
| *V*, Å$^3$ | 5982.0(1.0) | 5907.9(8) |
| *Z* | 4 | 4 |
| *ρ*, g cm$^{-3}$ | 1.861 | 1.937 |
| cryst size, mm$^3$ | 0.32 × 0.34 × 0.36 | 0.08 × 0.14 × 0.23 |
| *μ*, mm$^{-1}$ | 2.527 | 3.047 |
| data, restraints, params | 13644, 0, 794 | 13565, 0, 746 |
| final R1, wR2 | 0.0290, 0.0798 | 0.0567, 0.1450 |

explanation for why $Pr^{3+}$ is a more effective quencher of the Ru-based luminescence than is $Er^{3+}$ in these systems; an additional factor will be the slightly lower energy of $Pr^{3+}$-($^1D_2$) compared to that of $Er^{3+}$($^4S_{3/2}$), which will provide a greater thermodynamic gradient for the energy transfer in the former case. In fact, direct population of the $^1D_2$ level by the Ru → Pr energy transfer is demonstrated by the appearance of a Pr-based emission signal at 1010 nm, which is usually ascribed to the transition $^1D_2 \rightarrow {}^3F_4$.[18] Because the next highest energy level of $Pr^{3+}$ ($^3P_0$, at ≈ 21 000 cm$^{-1}$) is too high to act as an energy acceptor from the Ru unit, population of the $^1D_2$ level of $Pr^{3+}$ can only be achieved directly by an energy transfer from $[Ru(bipy)(CN)_4]^{2-}$. These considerations show that we can, therefore, rationalize well the observed order of energy-transfer rates of Nd > Pr > Er > Yb.

The lifetimes of the lanthanide-based luminescences were also measured and are included in Table 1. There were two difficulties here. First, in some cases, the lanthanide emission bands overlap with the tail end of the weak, residual Ru-based luminescence; this is a problem for $Yb^{3+}$ (980 nm) and $Pr^{3+}$ (840 and 1010 nm; see Figure 9). For Yb in particular, it appears that the Yb-based luminescence and the overlapping Ru-based luminescence are sufficiently similar that they cannot be separated. In **$Ru_2$YbK**, the Ru-based luminescence lifetime was measured at 700 nm to be 197 ns; at 980 nm, the luminescence decay can, in fact, be fitted reasonably well, assuming a single decay component of 197 ns, which applies to both. However, there is a rise-time component of 160 ns in the 980 nm luminescence that can be ascribed to the Ru → Yb energy transfer; the reciprocal of this gives an energy-transfer rate of 6 × 10$^6$ s$^{-1}$, rather higher than the value of 3 × 10$^6$ s$^{-1}$ that was estimated earlier from the Ru-based emission lifetime but not significantly so, given the approximations involved in fitting these luminescence decays to just one or two exponential components. Importantly, however, the main conclusion regarding the efficiency of the lanthanides at

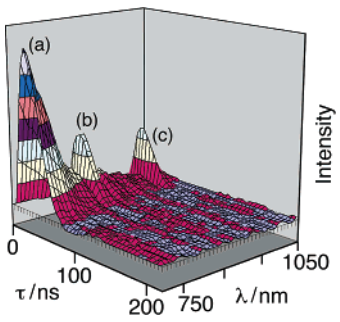


**Figure 9.** Time-resolved luminescence profile of **$Ru_2$PrK** in the region 750−1050 nm, showing overlap of the tail of the Ru-based emission (a) with the two Pr-based emission lines (b and c).

(18) Davies, G. M.; Aarons, R. J.; Motson, G. R.; Jeffery, J. C.; Adams, H.; Faulkner, S.; Ward, M. D. *Dalton Trans.* **2004**, 1136.

quenching the Ru-based excited state (Nd > Pr > Er > Yb) is not affected.

Factoring out the Ru-based component from the decay allowed an estimation of the $Pr^{3+}$ emission lifetime as 22 ns. At longer wavelengths, interference from Ru-based emission ceases to be a problem and the $Nd^{3+}$ lifetime, calculated from both the 1055 and 1340 nm signals, is 45 ns. For $Er^{3+}$, the signal at 1530 nm is so weak that a meaningful lifetime value could not be determined; we can say only that it is < 200 ns. In all of these cases, no rise time could be detected because of instrumental limitations.

The shortness of the lanthanide-based emission lifetimes in these systems is noteworthy. Despite the use of $D_2O$ ligands to eliminate the well-known quenching effects of OH oscillators,[15] the lifetimes are still much less than those usually seen for molecular complexes in non-hydroxylic solvents or in the solid state, and replacing coordinated $H_2O$ ligands by $D_2O$ in **$Ru_2YbK$** has surprisingly little effect. In our earlier communication,[11] the Yb-based emission lifetime in **$Ru_2YbK$** (crystallized from $H_2O$) was reported as 293 ns, with a coordination sphere containing six $H_2O$ and two cyanide ligands. Replacing the six water ligands by $D_2O$ (this work) has resulted in a Yb-based emission with a lifetime of (approximately) 197 ns. Given the difficulty in deconvoluting the Yb-based emission from the overlapping Ru-based emission, the difference between these two lifetimes is probably insignificant, but it is clear that replacing six $H_2O$ ligands with $D_2O$ ones has not significantly increased the luminescence lifetime in the expected manner, and the same is true for all of the other complexes.

The molecular complexes that we and others have investigated recently[2,5] have luminescence lifetimes of typically 10−15 $\mu$s for $Yb^{3+}$, 1 $\mu$s for $Nd^{3+}$, and 1−2 $\mu$s for $Er^{3+}$, when there no coordinated OH oscillators. Time-resolved studies on $Pr^{3+}$ are much rarer, but we measured lifetimes in the 50−100 ns range for a coordinatively saturated pyrazolylborate/diketonate complex recently in $CH_2Cl_2$ and $CD_3OD$.[18] In these molecular species, luminescence lifetimes in the solid state are always generally similar to those in (non-hydroxylic) solutions. The weakness of the lanthanide luminescence in the cyanide-bridged coordination oligomers and polymers reported in this paper must arise by efficient quenching from vibrations other than O−H. The only obvious candidate is the intense cyanide stretching vibration at ca. 2040 $cm^{-1}$, although why a relatively low-energy vibration (very similar in energy to O−D, which is an ineffective quencher) should have such a strong effect is not at the moment clear.

## Conclusions

Crystallization of $[Ru(bipy)(CN)_4]^{2-}$ with lanthanide cations from aqueous solutions has resulted in coordination networks with a range of structures containing Ru−CN−Ln bridges, in which the $^3$MLCT luminescence of the Ru unit is quenched by the lanthanide, resulting in sensitized NIR luminescences from $Yb^{3+}$, $Nd^{3+}$, $Pr^{3+}$, and $Er^{3+}$. Time-resolved luminescence measurements showed that the rate of the Ru → lanthanide energy transfer spans approximately 2 orders of magnitude, with the effectiveness of the lanthanide ions as quenchers (energy acceptors) being in the order Nd > Pr > Er > Yb. This order may be rationalized by considering the overlap of the lanthanide f−f transitions with the emission spectrum of the $[Ru(bipy)(CN)_4]^{2-}$ energy-donor unit. The luminescence lifetimes of the lanthanide centers are much shorter than those observed in molecular complexes, even when coordinated water ligands are replaced by $D_2O$, possibly because of quenching by vibrations from the coordinated cyanide ligands.

**Table 3.** Selected Bond Distances in the Metal Coordination Spheres[a]

| | | | |
|---|---|---|---|
| $[\{Ru(bipy)(CN)_4\}_2\{Pr(H_2O)_7\}\{K(H_2O)_2\}]\cdot 10H_2O$ | | | |
| Pr(1)−N(16) | 2.538(6) | K(1)−C(15) | 3.246(7) |
| Pr(1)−O(1) | 2.542(6) | K(1)−N(15) | 3.056(7) |
| Pr(1)−O(2) | 2.483(5) | K(1)−N(16) | 3.046(6) |
| Pr(1)−O(3) | 2.499(9) | K(1)−C(16) | 3.202(6) |
| Pr(1)−O(4) | 2.620(7) | K(1)−O(7) | 2.853(10) |
| Pr(1)−O(5) | 2.572(8) | K(1)−O(6) | 2.865(13) |
| $[\{Ru(bipy)(CN)_4\}_2\{Er(H_2O)_6\}\{K(H_2O)_4\}]\cdot 5H_2O$ | | | |
| Er(1)−O(106) | 2.338(4) | K(1)−O(105) | 3.031(5) |
| Er(1)−O(105) | 2.341(4) | K(1)−O(106) | 3.222(5) |
| Er(1)−O(102) | 2.343(5) | K(1)−O(107) | 2.840(6) |
| Er(1)−O(101) | 2.351(6) | K(1)−O(108) | 2.882(7) |
| Er(1)−O(104) | 2.384(6) | K(1)−O(109) | 2.846(7) |
| Er(1)−O(103) | 2.386(5) | K(1)−O(110) | 2.801(8) |
| Er(1)−N(132) | 2.391(6) | K(1)−N(132A) | 3.344(7) |
| Er(1)−N(116) | 2.410(6) | K(1)−N(116A) | 3.360(7) |
| Er(2)−O(1) | 2.399(5) | O(5)−K(2) | 3.403(6) |
| Er(2)−O(2) | 2.326(5) | O(6)−K(2) | 2.964(5) |
| Er(2)−O(3) | 2.405(5) | O(7)−K(2) | 2.787(6) |
| Er(2)−O(4) | 2.375(6) | O(8)−K(2) | 2.900(6) |
| Er(2)−O(5) | 2.319(5) | O(9)−K(2) | 2.778(7) |
| Er(2)−O(6) | 2.354(4) | O(10)−K(2) | 2.857(6) |
| Er(2)−N(32) | 2.369(6) | K(2)−N(16A) | 3.331(7) |
| Er(2)−N(16) | 2.429(6) | K(2)−N(32A) | 3.303(7) |
| Er(1)−K(1) | 4.380(2) | Er(2)−K(2) | 4.415(2) |
| Er(1)−K(1A) | 4.267(2) | Er(2)−K(2A) | 4.247(2) |
| $[\{Ru(bipy)(CN)_4\}_3\{Gd(H_2O)_4\}_2]\cdot 11H_2O$ | | | |
| Gd(1)−N(58) | 2.461(7) | Gd(2)−O(8) | 2.338(6) |
| Gd(1)−O(3) | 2.409(7) | Gd(2)−O(7) | 2.414(6) |
| Gd(1)−O(1) | 2.439(13) | Gd(2)−O(5) | 2.418(6) |
| Gd(1)−N(39A) | 2.448(8) | Gd(2)−O(6) | 2.436(6) |
| Gd(1)−O(4) | 2.450(5) | Gd(2)−N(57C) | 2.462(8) |
| Gd(1)−O(2) | 2.481(6) | Gd(2)−N(25C) | 2.469(7) |
| Gd(1)−O(1B) | 2.485(19) | Gd(2)−N(24A) | 2.501(7) |
| Gd(1)−N(41) | 2.412(8) | Gd(2)−N(42) | 2.446(7) |
| $[\{Ru(bipy)(CN)_4\}_3\{Nd(H_2O)_4\}_2]\cdot 11H_2O$ | | | |
| Nd(1)−N(25) | 2.493(3) | Nd(2)−O(7) | 2.425(3) |
| Nd(1)−N(42) | 2.531(3) | Nd(2)−O(5) | 2.488(3) |
| Nd(1)−O(2) | 2.405(9) | Nd(2)−O(8) | 2.491(3) |
| Nd(1)−O(3) | 2.475(3) | Nd(2)−O(6) | 2.499(3) |
| Nd(1)−O(1) | 2.524(3) | Nd(2)−N(58D) | 2.506(3) |
| Nd(1)−N(55B) | 2.532(3) | Nd(2)−N(24C) | 2.550(3) |
| Nd(1)−O(4) | 2.554(3) | Nd(2)−N(41) | 2.533(3) |
| Nd(1)−O(2A) | 2.607(13) | Nd(2)−N(26) | 2.521(3) |

[a] The $[Ru(bipy)(CN)_4]^{2-}$ units in every case have unremarkable geometries with Ru−C distances of 1.95−2.05 Å and Ru−N distances of ca. 2.1 Å.

## Experimental Section

**Syntheses.** Slow evaporation of an aqueous solution of $K_2[Ru(bipy)(CN)_4]$ and lanthanide chloride hydrate (Ln = Pr, Nd, Gd, Er, Yb) in a 2:1 ratio, over a period of 2−3 weeks, resulted in a crop of crystals in varying yields of up to 80%; these were filtered off and air-dried. Elemental analyses, in all cases, indicated the presence of several lattice water molecules in addition to the expected water ligands coordinated to the $Ln^{3+}$ centers, in agreement

with the crystal structures, although in some cases, the number of water molecules detected by analysis was less than that found in the crystal structure, indicating a partial loss of lattice water molecules on drying the crystals. IR spectra were recorded as powders using a diamond-ATR cell on a Perkin−Elmer Paragon FTIR spectrometer. [{Ru(bipy)(CN)$_4$}$_2${Yb(H$_2$O)$_6$}{K(H$_2$O)$_4$}]·5H$_2$O was prepared and characterized as described earlier.

**[{Ru(bipy)(CN)$_4$}$_2${Pr(H$_2$O)$_7$}{K(H$_2$O)$_2$}]·9H$_2$O.** Found: C, 27.7; H, 3.9; N, 13.2%. Calcd: C, 27.4; H, 4.3; N, 13.7%. (The crystal structure has 10H$_2$O.) IR ($\nu$, cm$^{-1}$): 3343 (br, s), 2485 (br, w), 2113 (w), 2037 (s), 1600 (m), 1468 (m), 1444 (m), 1428 (m), 1312 (w), 1242 (w), 1157 (w), 763 (s), 734 (m).

**[{Ru(bipy)(CN)$_4$}$_2${Er(H$_2$O)$_6$}{K(H$_2$O)$_4$}]·4H$_2$O.** Found: C, 28.2; H, 3.4; N, 14.1%. Calcd: C, 28.5; H, 3.8; N, 14.2%. (The crystal structure has 5H$_2$O.) IR ($\nu$, cm$^{-1}$): 3380 (br, s), 2501 (br, m), 2097 (m), 2040 (s), 1599 (m), 1468 (m), 1441 (m), 1421 (m), 1311 (w), 1242 (w), 1152 (w), 763 (s), 733 (m).

**[{Ru(bipy)(CN)$_4$}$_3${Nd(H$_2$O)$_4$}$_2$]·11H$_2$O.** Found: C, 29.3; H, 3.3; N, 14.7%. Calcd: C, 29.4; H, 3.6; N, 14.7%. IR ($\nu$, cm$^{-1}$): ∼3600 (sh), 3290 (br, m), 2100 (m), 2046 (s), 1599 (m), 1468 (m), 1444 (m), 1421 (m), 1312 (w), 1241 (w), 766 (s), 732 (m).

**[{Ru(bipy)(CN)$_4$}$_3${Gd(H$_2$O)$_4$}$_2$]·10H$_2$O.** Found: C, 28.6; H, 3.2; N, 14.2%. Calcd: C, 29.0; H, 3.6; N, 14.5%. (The crystal structure has 11H$_2$O.) IR ($\nu$, cm$^{-1}$): ∼3600 (sh), 3290 (br, m), 2100 (m), 2046 (s), 1599 (m), 1468 (m), 1444 (m), 1421 (m), 1312 (w), 1242 (w), 766 (s), 732 (m).

**X-ray Crystallography.** Suitable crystals were mounted on a Bruker SMART-CCD diffractometer equipped with graphite-monochromatized Mo Kα radiation. Details of the crystal, data collection, and refinement parameters are summarized in Table 2, and selected structural parameters are collected in Table 3. After integration of the raw data and merging of the equivalent reflections, an empirical absorption correction was applied on the basis of a comparison of multiple symmetry-equivalent measurements.[19] The structures were solved by direct methods and refined by full-matrix least squares on weighted $F^2$ values for all reflections using the SHELX suite of programs.[20] None of the refinements presented any significant problems. For coordinated and lattice water molecules, H atoms were added only when both of them showed up clearly in a refinement using only low-angle data; they were then fixed in position with O−H distances of 0.85 Å. In **Ru$_2$PrK**, the two water ligands on the K$^+$ ion, O(6) and O(7), were both disordered over two positions with fractional site occupancies of 50% in each site.

**Luminescence Measurements.** Luminescence measurements were made using powdered samples packed against a quartz window in a specially prepared die. Steady-state measurements were made using a Perkin−Elmer LS-55 spectrometer, fitted with a front surface accessory. For time-resolved and NIR measurements, the whole assembly was held with the plane of the window at 30° to the incident radiation from a dye laser pumped by a pulsed nitrogen laser (PTI-3301). Light emitted at right angles to the excitation beam was focused onto the slits of a monochromator (PTI-120), which was used to select the appropriate wavelength. The growth and decay of the luminescence at selected wavelengths were detected using a germanium photodiode (Edinburgh Instruments, EI−P) and recorded using a digital oscilloscope (Tektronix TDS220) before being transferred to a PC for analysis. Luminescence lifetimes were obtained by iterative reconvolution of the detector response (obtained by using a scatterer) with exponential components for growth and decay of the metal-centered luminescence, using a spreadsheet running in Microsoft Excel. The details of this approach have been discussed elsewhere.[21]

**Acknowledgment.** We thank the EPSRC (UK) and the University of Sheffield for financial support.

**Supporting Information Available:** A CIF file containing details of the four crystal structures in the paper. This material is available free of charge via the Internet at http://pubs.acs.org.

IC050512K

(19) Sheldrick, G. M. *SADABS*; University of Göttingen: Göttingen, Germany, 1996.

(20) *SHELXTL*, version 5.1; Bruker Analytical X-ray Instruments Inc.: Madison, WI, 1998.

(21) Beeby, A.: Faulkner, S. *Chem. Phys. Lett.* **1997**, *266*, 116.